Effects of Gas Pressure on the Size Distribution and Structure of Carbon Nanoparticles Using Ar + CH_4 Multi-Hollow Discharged Plasma Chemical Vapor Deposition*)

Sung Hwa HWANG, Kunihiro KAMATAKI, Naho ITAGAKI, Kazunori KOGA and Masaharu SHIRATANI

Department of Electronics, Kyushu University, Fukuoka 819-0395, Japan

(Received 1 January 2019 / Accepted 1 April 2019)

Using an Ar + CH_4 multi-hollow discharge plasma chemical vapor deposition (MHDPCVD) method, carbon nanoparticles (CNPs) are synthesized in a size range between 10 nm and 100 nm at gas pressures from 2 Torr to 5 Torr. The size of the nanoparticles increases from 45.42 nm^3 at 2 Torr to 67.85 nm^3 at 5 Torr. The size dispersion also increases. Conversely, the optical emission intensities and generation of carbon related radicals decrease with increasing pressure. The Raman measurements indicate that these CNPs are composed of polymer structures containing relatively high clustered and distorted sp2 sites.

Keywords: carbon nanoparticle, multi-hollow discharge plasma chemical vapor deposition, optical emission spectroscopy, Raman spectroscopy

DOI: 10.1585/pfr.14.4406115

1. Introduction

Carbon nanomaterials (CNPs) have been widely employed in basic research and applications due to their many beneficial characteristics including their mechanical, chemical, and electrical properties [1–3]. Of the various carbon nanomaterials, nanoparticles are one of the most prominent nanotechnologies. Nanoparticles often involve not only the features of their base materials but also nanoscale effects, including unique and attractive properties of nanoparticles that are dramatically different from those of bulk materials. The properties of nanoparticles are highly sensitive to their size, structure, and composition [4–12].

So far, researchers have applied multiple methods to synthesize CNPs. However, most of these methods have potential drawbacks, showing unfavorable reaction conditions, such as a lack of aqueous solubility, prolonged reaction durations, and the usage of dispersants, resulting in difficulties in controlling the size and amount of CNPs produced. In particular, the lack of uniformity for practical usage in advanced applications may lead to significant limitations [13–17]. Plasma processes are a promising method of producing CNPs without contamination. This type of process controls the coagulation of nanoparticles via the ratio of the particle density to the particle charge [18]. We have studied Si nanoparticle generation using multi-hollow discharge plasma chemical vapor deposition (MHDPCVD), which controls nanoparticle generation and growth via the gas residence time, leading to the continuous synthesis of carbon nanoparticles [19–22].

In this study, we applied Ar and CH_4 gases to the MHDPCVD method to synthesize size-controlled carbon nanoparticles and examined their deposition onto substrates.

2. Experimental

Figure 1 shows a schematic diagram of the MHDPCVD reactor. A power electrode with eight 0.5-cm diameter holes was installed in the reactor. The electrode was sandwiched by two grounded electrodes that had eight

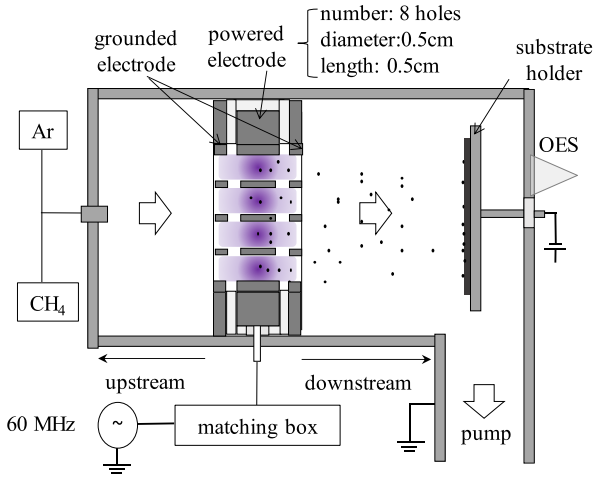

Fig. 1 Schematic diagram of the MHDPCVD.

author's e-mail: sh.hwang@plasma.ed.kyushu-u.ac.jp

*) This article is based on the presentation at the 2nd Asia-Pacific Conference on Plasma Physics (AAPPS-DPP2018).

holes at the same positions as the powered electrode. Then, the Ar and CH_4 gases were introduced, passed through the holes, and evacuated via a pump system. Plasma was primarily generated in the holes by applying RF voltages to the powered electrode. CNPs were generated in the discharge and transported toward the downstream of the discharge by the gas flow [9]. They were sampled on Si substrates and mesh grids for analysis via transparent electron microscopy (TEM) on the substrate holder located 10 cm from the electrodes.

The sampled CNPs were observed using high resolution TEM (JEOL, JEM-2010) to measure their size distribution. To understand the mechanism of the CNP generation, optical spectra were measured with an optical emission spectroscope (Ocean Optics, USB2000+) [23]. The structure of the deposit on the substrates was measured using a Raman spectroscope with a green laser (Jasco, NRS-3000; λ = 532 nm).

The experimental conditions consisted of a mixture of Ar and CH_4 gas with a 6:1 ratio that was introduced at 100 sccm. The gas pressure was controlled to be from 1 Torr to 5 Torr. The discharge frequency and power were 60 MHz and 40 W, respectively. The substrates were grounded, and their temperature was that of the room temperature. The discharge duration was 90 min.

3. Results and Discussion

Figure 2 shows TEM images of CNPs deposited on TEM grids as a parameter of the working pressure. For 1 Torr and 1.5 Torr, no CNPs are observed; however, CNPs are deposited uniformly on the grids above 2 Torr. As the pressure increases, the number of particles decreases and the size of the particles gradually increases. This indicates that we succeeded in the continuous synthesis of CNPs using the high-pressure Ar + CH_4 MHDPCVD method. Figure 3 illustrates the size distribution of the deposited CNPs. The mean volume of the CNPs decreases from 67.85 nm^3 at 5 Torr to 45.42 nm^3 at 2 Torr. The size dispersion is between 15 nm and 100 nm, and the population of the bigger size is larger at higher pressure than at lower pressure.

To obtain information about radical generation, we measured the optical emission spectroscopy (OES) spectra of the discharges. Figure 4 shows a typical OES spectrum, in which un-ionized argon (Ar I), hydrogen (Balmer lines,

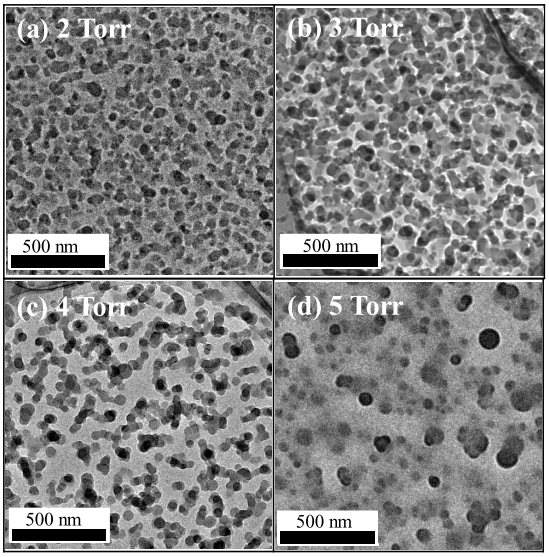

Fig. 2 TEM images of deposited CNPs as a parameter of the pressure.

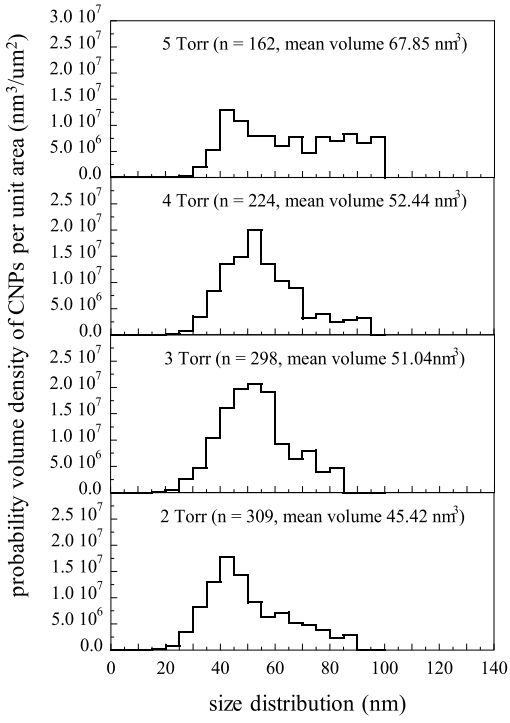

Fig. 3 CNPs size distribution for gas pressures between 2 Torr (bottom) and 5 Torr (top).

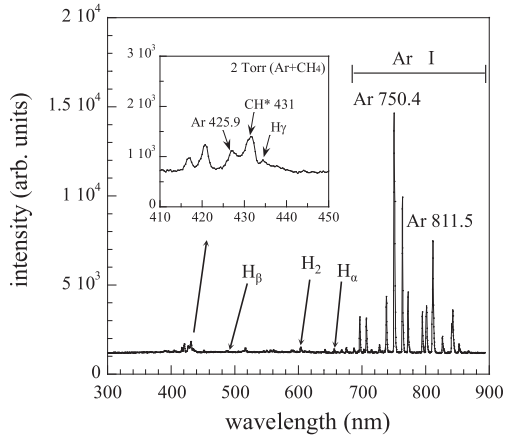

Fig. 4 Typical optical emission spectrum of the Ar + CH_4 multi-hollow discharge plasma.

H_α at 656 nm, H_β at 486 nm, and $H\gamma$ at 434 nm), hydrogen molecules (H_2), and CH* radicals (432.6 nm) are emitted from the discharge [24–30]. Figure 5 shows the pressure dependence of the emission intensity of CH* (432.6 nm). The intensity rapidly decreases with increasing pressure. This result indicates that the generation rate of carbon related radicals, which are the precursors of CNP production, is smaller for higher pressures.

A possible key factor that determines the CNP size is the gas residence time, which is obtained by dividing the velocity of gas passing through the plasma discharge zone by the distance from the electrode. During the process, fresh gases enter from the left side of the hollow in Fig. 1. The gas molecules are transported toward the exit of the hollow by the gas flow velocity. During this transport, gas molecules are dissociated via electron collision and then radicals are generated. The particles are nucleated by the successive polymerization of the radicals. The nucleated particles grow via the deposition of the radicals or via coagulation with other particles. Their growth stops outside the hollows. Therefore, the gas residence time in the hollows is key to determining the sizes of the nanoparticles [20–22].

Even though the generation rate of carbon related radicals decreases with increasing pressure, more radicals can be deposited on nucleated nanoparticles due to the longer gas residence time in the plasma discharge region. For 1 Torr and 1.5 Torr, no CNPs are deposited. This might be due to the fact that smaller nanoparticles are generated but cannot be deposited on the substrate. The gas flow line abruptly changes direction in front of the substrate holder. Larger-sized CNPs can be transported toward the substrates due to their large inertia. For 1 Torr and 1.5 Torr, the generated nanoparticles might be transported to the pump system.

The Raman spectra collected from the CNPs deposited on the Si substrates as a function of the pressure is illustrated in Fig. 6. For all pressures, two peaks corresponding to the D band (1350 cm^{-1}) and the G band (1580 cm^{-1}) are observed. In general, carbon films formed by a plasma CVD process represent amorphous structures including sp2 and sp3 bonding. Therefore, the produced CNPs might be hydrogenated amorphous carbon (a-C:H) [31–33]. The peak intensities at 3 Torr and 4 Torr are larger than those at the other pressures. For 1 Torr and 1.5 Torr, where nanoparticles were not observed, these peaks might correspond to a-C:H films deposited by a small amount of transported radicals from the discharge.

Figure 7 shows the pressure dependence of the intensity ratio of the D band and the G band, I_D/I_G, the full width at half maximum (FWHM) of the G band, and the peak position of the G band. The Raman spectrum of diamond-like carbon highly depends on the clustering and disorder of the sp2 sites and only indirectly on the fraction of sp3 sites [34–38]. The ratio of I_D/I_G, which is a general indicator for the zone edges or photons of the carbon clusters, depends on the cluster size and distribution [35, 39]. Another measure of disorder is the bandwidth of the G band, which is related to distortions within each sp2 cluster and is proportional to the stress and the sp3 fraction in the DLC films. The G band position originates from the convolution of a typical sp2 carbon around 1580 cm^{-1}; however, the G band around 1600 cm^{-1} occurs due to the high frequency edge of the graphitic density of states [38–40]. In the case of the absence of nanoparticles (1 Torr and 1.5 Torr), the I_D/I_G ratio was approximately 0.5, FWHM was approximately 150 cm^{-1}, and the G band position was from 1600 cm^{-1} to 1610 cm^{-1}. These values indicate low clustered sp2 sites,

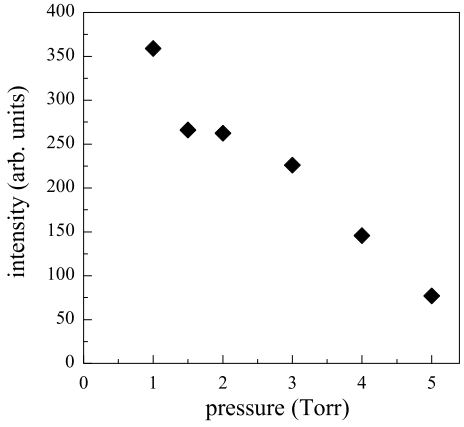

Fig. 5 Intensity of the CH*(431) emission spectra between 1 Torr and 5 Torr.

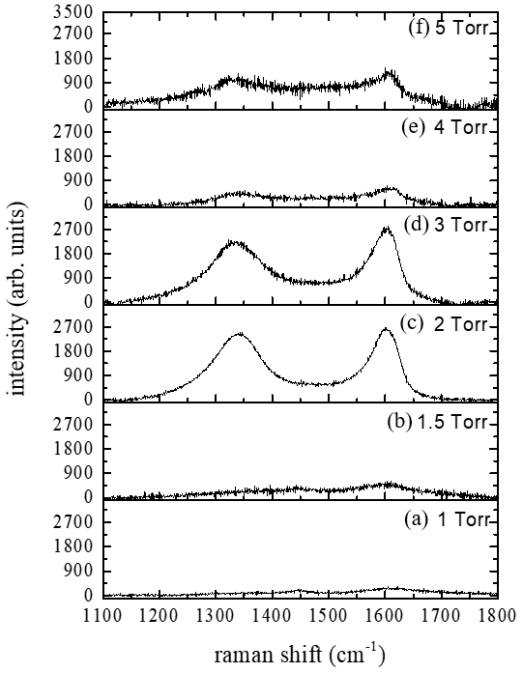

Fig. 6 Raman spectra of deposits on Si substrates as a function of the gas pressure.

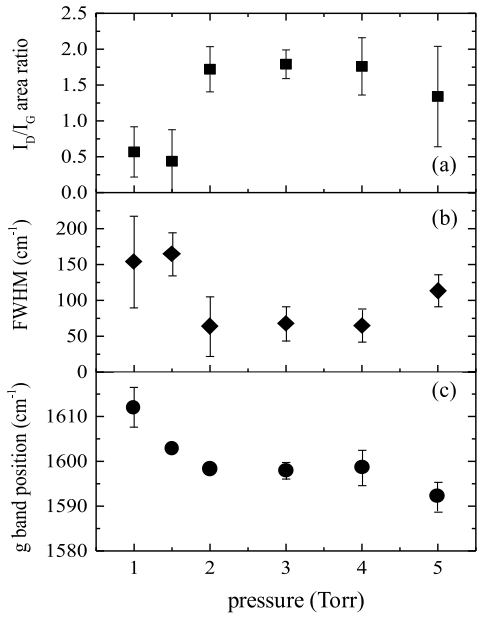

Fig. 7 Structure analysis of CNPs via the Raman spectra: (a) the I_D/I_G ratio, (b) FWHM, and (c) the G band position.

distortions within each sp2 cluster proportional to the high stress, and bond-angle disorder. Conversely, with the existence of carbon nanomaterials (2 - 5 Torr), the I_D/I_G ratio was over 1.5, FWHM was approximately 60 cm^{-1}, and the G band position was less than 1600 cm^{-1}. These values show that the CNP deposition case represents high sp2 bonded clusters, distortions, and low bond angle disorder. These results clearly show the differences between cases with and without CNPs.

4. Conclusions

We succeeded in continuously synthesizing CNPs using a high-pressure Ar + CH_4 MHDPCVD method. With an increase in pressure from 1 Torr to 5 Torr, CNPs were observed at pressures above 2 Torr with sizes between 10 nm and 100 nm. The mean size of the CNPs increased with increasing pressure. The TEM and OES results suggest that controlling the gas residence time in the plasma is the key parameter. The Raman measurements indicate that the CNPs are polymer structures that are thought to contain relatively high clustered and distorted sp2 sites.

Acknowledgments

This study was partly supported by JSPS KAKENHI KAKENHI Grant Number JP26246036.

[1] P. Greil, Advanced Engineering Acta **17**, 002 (2015).
[2] Y. Zhao, M. Liu, X. Deng, L. Miao, P.K. Tripathi, X. Ma, D. Zhu, Z. Xu, Z. Hao and L. Gan, Electrochimica Acta **153**, 448 (2015).
[3] L. Xiao, Y. Cao, W.A. Henderson, M.L. Sushko, Y. Shao, J. Xiao, W. Wang, M.H. Engelhard, Z. Nie and J. Liu, Nano Energy **19**, 279 (2016).
[4] Y. Watanabe, M. Shiratani, Y. Kubo, I. Ogawa and S. Ogi, Appl. Phys. Lett. **53**, 1263 (1988).
[5] A.T. Bell, Science **299**, 1688 (2003).
[6] H. Häkkinen, Nat. Chem. **4**, 443 (2012).
[7] Z. Nie, A. Petukhova and E. Kumacheva, Nat. Nano. **5**, 453 (2010).
[8] M. Shiratani, T. Kakeya, K. Koga, Y. Watanabe and M. Kondo, Trans. Mater. Res. Soc. Jpn. **30**, 307 (2005).
[9] K. Koga, S. Iwashita and M. Shiratani, J. Phys. D **40**, 2267 (2007).
[10] G. Uchida, K. Yamamoto, Y. Kawashima, M. Sato, K. Nakahara, K. Kamataki, N. Itagaki, K. Koga, M. Kondo and M. Shiratani, Phys. Status Solidi C **8**, 3017 (2011).
[11] Y. Kim, K. Hatozaki, Y. Hashimoto, G. Uchida, K. Kamataki, N. Itagaki, H.W. Seo, K. Koga and M. Shiratani, Jpn. J. Appl. Phys. **52**, 01AD01 (2013).
[12] M. Shiratani, K. Koga, K. Kamataki, S. Iwashita, G. Uchida, H. Seo and N. Itagaki, Jpn. J. Appl. Phys. **53**, 010201 (2014).
[13] V. Roshni and D. Ottoor, J. Lumin. **161**, 117 (2015).
[14] H. Zhu, X. Wang, Y. Li, Z. Wang, F. Yang and X. Yang, Chem. Commun. Issue 34, 5118 (2009). DOI: 10.1039/b907612c
[15] X. Sun and Y. Li, Angew. Chem. **43**, 597 (2004).
[16] A.B. Fuertes, M. Sevilla, T. Valdes-Solis and P. Tartaj, Chem. Mater. **19**, 5418 (2007).
[17] H. Li, X. He, Y. Liu, H. Huang, S. Lian, S. Lee and Z. Kang, Carbon **49**, 605 (2011).
[18] K. Koga, Y. Matsuoka, K. Tanaka, M. Shiratani and Y. Watanabe, Appl. Phys. Lett. **77**, 196 (2000).
[19] T. Kojima, S. Toko, K. Tanaka, H. Seo, N. Itagaki, K. Koga and M. Shiratani, Plasma Fusion Res. **13**, 1406082 (2018).
[20] M. Shiratani, K. Koga, S. Iwashita, G. Uchida, N. Itagaki and K. Kamataki, J. Phys. D **44**, 174038 (2011).
[21] S. Toko, Y. Torigoe, K. Keya, T. Kojima, H. Seo, N. Itagaki, K. Koga and M. Shiratani, Surf. Coat. Technol. **326**, 388 (2017).
[22] W.M. Nakamura, Y. Kawashima, M. Tanaka, H. Sato, J. Umetsu, H. Miyahara, H. Matsuzaki, K. Koga and M. Shiratani, J. Plasma Fusion Res. **8**, 736 (2009).
[23] N.A. Sanchez, C. Rincon, G. Zambrano, H. Galindo and P. Prieto, Thin Solid Films **373**, 247 (2000).
[24] F. Sohbatzadeh, R. Safari, G.R. Etaati, E. Asadi, S. Mirzanejhad, M.T. Hosseinnejad, O. Samadi and H. Bagheri, Superlatties Microstruct. **89**, 231 (2016).
[25] X. Bian, Q. Chen, Y. Zhang, L. Sang and W. Tang, Surf. Coat. Technol. **202**, 5383 (2008).
[26] A.M. Daltrini, M. Sevilla, T. Valdes-Solis and P. Tartaj, J. Appl. Phys. **101**, 073309 (2007).
[27] X. Dong, K. Koga, D. Yamashita, H. Seo, N. Itagaki, M. Shiratani, Y. Setsuhara, M. Sekine and M. Hori, Trans. Mater. Res. Soc. Jpn. **40[2]**, 123 (2015).
[28] Y.K. Lee and C.W. Chung, J. Appl. Phys. **109**, 013306 (2011).
[29] A. Pastol and Y. Catherine, J. Phys. D. **23**, 799 (1990).
[30] D.L. Gerrard and W.F. Maddam, Appl. Spectrosc. Rev. **22(2 & 3)**, 251 (1986).
[31] N. Everall and B. King, Macromol. Symp. **141**, 103 (1999).
[32] H.D. Wagner, Polymer-Carbon Nanotube Composites, eds. by P. Pötschke and T. McNally (Woodhead Publishing Limited, 2011) p.400. ISBN: 9781845697617
[33] H. Dai, Phys. Status Solidi A **210**, No9, 1874 (2013).
[34] J. Robertson, Mater. Sci. Eng. **R37**, 129 (2002).

[35] C.A. Freyman, Y. Chen and Y.W. Chung, Surf. Coat. Technol. **201**, 164 (2006).
[36] Z. Xu, Y.J. Zheng, F. Jiang, Y.X. Leng, H. Sun and N. Huang, Appl. Surface Sci. **264**, 207 (2013).
[37] C. Wei, Y.S. Wang and F.C. Tai, Diam. Relat. Mater. **18**, 407 (2009).
[38] N. Dwivedi, S. Kumar, R.K. Tripathi, J.D. Carey, H.K. Malik and M.K. Dalai, ACS Appl. Mater. Interf. **4**, 5309 (2012).
[39] S.B. Singh, M. Pandey, N. Chand, A. Biswas, D. Bhattacharya, S. Dash, A.K. Tyagi, R.M. Dey, S.K. Kulkarni and D.S. Patil, Bull. Mater. Sci. **31**, 813 (2008).
[40] V.I. Korepanov, H. Hamaguchi, E. Osawa, V. Ermolenkov, I.K. Lednev, B.J.M. Etzold, O. Levinson, B. Zousman, C.P. Epperla and H.C. Chang, Carbon **121**, 322 (2017).